JOURNAL OF EXPERIMENTAL ZOOLOGY 297A:1–16 (2003)

Mitochondrial Distribution and Glycogen Dynamics Suggest Diffusion Constraints in Muscle Fibers of the Blue Crab, *Callinectes sapidus*

KIM-LAURA BOYLE, RICHARD M. DILLAMAN, AND STEPHEN T. KINSEY*
Department of Biological Sciences, University of North Carolina at Wilmington, 601 South College Road, Wilmington, North Carolina 28403–5915

ABSTRACT The scaling of mitochondrial distribution, citrate synthase activity, and post-contractile glycogen recovery was examined in muscle fibers of the blue crab, *Callinectes sapidus*. The fast-twitch muscle fibers of *C. sapidus* can reach extremely large dimensions, which may impose constraints on aerobic metabolic processes. However, muscle cells from small crabs are not giant, meaning that during development muscle fibers cross and greatly exceed the surface area to volume (SAV) and diffusion threshold that is adhered to by the cells of most organisms. Cell diameters in the smallest size class were $\simeq$100 μm, while the largest size class had cell diameters in excess of 500 μm. In the smallest cells, the fractional area of subsarcolemmal and intermyofibrillar mitochondria was similar. However, in the largest cells, mitochondria were almost exclusively subsarcolemmal. Total fractional area of mitochondria was highest in the largest cells due to a proliferation of subsarcolemmal mitochondria. In contrast, citrate synthase activity decreased as cell size increased. Following burst contractile activity, glycogen concentrations decreased significantly and remained depressed for several hours in muscle comprised of giant cells, consistent with previous findings that anaerobic glycogenolysis fuels certain components of post-contractile recovery. However, in muscle composed of the smallest muscle cells, glycogen levels did not decrease significantly following burst activity. While normal scaling of aerobic metabolism would predict a slower aerobic recovery in larger animals, the present results suggest that cellular organization, SAV, and intracellular diffusion distances also impose constraints on aerobic processes in *C. sapidus*. *J. Exp. Zool. 297A: 1–16, 2003.* © 2003 Wiley-Liss, Inc.

INTRODUCTION

The blue crab, *Callinectes sapidus*, is an efficient swimmer that exhibits both sustainable, aerobic locomotion and burst-escape locomotion to avoid predators (reviewed in Booth and McMahon, '92). Both types of locomotion are powered by the fifth pereiopod, which has been extensively modified to a paddle-like shape that makes it well adapted for swimming (White and Spirito, '73). The blue crab's swimming leg muscle is similar to that of many fish, in that it consists of a small, dark region of aerobic fibers that power sustainable swimming, surrounded by a large mass of anaerobic fibers used for burst swimming (Tse et al., '83). An unusual property of the anaerobic, white muscle fibers of large crustaceans like the blue crab is the extreme range of cell sizes the animal will possess during its lifetime. Due to constraints placed on cellular dimensions by surface area to volume (SAV) and diffusion distances, it is generally acknowledged that there is a maximum diameter for cells of approximately 100 μm (Russell et al., 2000). However, while juvenile crustaceans likely have muscle cells $<$100 μm in diameter, the fibers of large adult crustaceans, including those of the blue crab, regularly reach diameters well beyond the perceived 100 μm limit and can even exceed 500 μm in diameter (Hoyle and Smyth, '63, Tse et al., '83).

Giant cells are not unusual in nature. The giant axons of squid and other organisms have offered insights into how the physical principles of cable theory can be applied to neuronal function (reviewed in Dorsett, '80). Giant axons are typically associated with rapid escape responses in a variety of organisms, including crustaceans

Grant sponsor: National Science Foundation; Grant number: DBI–99–78613.
*Correspondence to: Stephen T. Kinsey, Department of Biological Sciences, University of North Carolina at Wilmington, 601 South College Road,Wilmington, NC, 28403–5915.
E-mail: kinseys@uncw.edu
Received 8 May 2002; Accepted 18 November 2002
Published online in Wiley InterScience (www.interscience.wiley.com). DOI:10.1002/jez.a.10227

© 2003 WILEY-LISS, INC.

(Newland et al., '92), and their extreme diameters serve to enhance the rate of propagation of action potentials (reviewed in Gilbert et al., '90). However, giant muscle fibers do not appear to confer a similar functional advantage. In fact, certain muscle cells of the barnacle, *Balanus nubilus*, which are among the largest known cells (up to 5 mm in diameter), have some properties that are characteristic of slow-twitch fibers (Hoyle, '87). While crustacean giant muscle cells have been used extensively in membrane physiology experiments because their large size allows for easy manipulation, (e.g. Hoyle and Smyth, '63; Ashley, '67, '78; Atwood, '73; Weiss et al., 2001), very little is known about their function in the animal or what limitations they may impose. In his review of the giant muscle cells of barnacles, Hoyle ('87) concluded that these giant muscle cells create no apparent advantage, and they may actually create functional difficulties.

Another unique morphological feature of crustacean muscle fibers, which is likely linked to their extreme diameter, is the presence of clefts or invaginations of the sarcolemma (Peachy, '67). The surface of crustacean muscle fibers is extensively invaginated to create subdivisions such that no portion of the contractile proteins are more than 20–50 μm from membrane that is continuous with the sarcolemma (Selverston, '67). These invaginations increase the surface area of the fiber and function to permit all parts of the muscle to contract at the same time, a function analogous to the T-tubules in mammalian muscle (Selverston, '67). However, while the smallest subdivisions have dimensions typical of ''normal'' cells, these divisions are discontinuous and the subdivisions remain interconnected, so that the fiber retains an effective diameter of several hundred microns (Rosenbluth, '69). In addition, histochemical work by Tse et al. ('83) showed that in white muscle of the adult blue crab, mitochondria are found almost exclusively at the periphery of the fiber (subsarcolemmal mitochondria). Thus, fast-twitch fibers from adult blue crabs have a thin peripheral cylinder of oxidative potential with a diameter of several hundred microns, meaning that the fibers are ''metabolically giant.'' Since the giant fibers of blue crabs are used exclusively for burst contraction and rely upon phosphagen hydrolysis and anaerobic glycogenolysis to supply ATP (England and Baldwin '83, '85), the large cellular dimensions should not impact the contraction process. However, a likely functional consequence of giant cell size is a reduced capacity for oxidative metabolism, including the aerobically fueled, post-contractile recovery process. The recovery process in crustacean muscle is, in fact, markedly different from that of vertebrate muscle following similar types of exercise. After exhaustive anaerobic exercise, vertebrate muscle undergoes a relatively rapid aerobic recovery of the phosphagen creatine phosphate (CP), which allows subsequent, high-force contractions (e.g. Kushmerick, '83; Meyer et al., '84; Curtain et al., '97; Meyer, '88). Following burst exercise in crustaceans, recovery must also occur quickly so that the animals can escape again if necessary. The recovery of the crustacean phosphagen, arginine phosphate (AP) is also surprisingly fast, and can occur within 20 minutes of exhaustive exercise (Head and Baldwin, '86; Thébault et al., '87). However, in crustaceans, the recovery of AP pools is primarily fueled by anaerobic glycogenolysis, which is reflected by the post-contraction buildup of lactate and depletion of glycogen (England and Baldwin, '83; Booth and McMahon, '85). This process is followed by a very slow, aerobic recovery that returns pH, glycogen stores, and lactate levels to pre-exercise states (Ellington, '83; Kamp, '89; Milligan et al., '89; Henry et al., '94). This pattern of recovery may represent one of the functional compromises of giant cell size that was alluded to by Hoyle ('87).

The present study examined the scaling of metabolic properties of anaerobic swimming leg muscle in *C. sapidus,* which has a post-metamorphic body mass range of more than three orders of magnitude. The burst contraction function of the white swimming leg muscles remains constant throughout development, despite the fact that during growth, fiber dimensions cross the approximate SAV and diffusion threshold of 100 μm. Therefore, metabolic reorganization and the functional consequences associated with cells becoming giant are of principle interest in this study. To address this issue, mitochondrial distribution, oxidative enzyme activity, and post-contractile glycogen dynamics were investigated not only as a function of body mass, but also in the context of cellular dimensions.

Three general effects of increased cellular dimensions were expected. First, cells of approximately 100 μm diameters, i.e. ''normal'' dimensions, would have both intermyofibrillar and subsarcolemmal distributions of mitochondria, typical of most cells. However as cells increased in size it was predicted that subsarcolemmal mitochondria would become dominant. Second,

both mitochondrial fractional area and aerobic enzyme activity would scale negatively with increased body mass, but with a steeper slope than predicted from normal patterns of metabolic scaling. Lastly, the time course of aerobic glycogen recovery following exhaustive, burst exercise would be slower in muscle from large animals, but more so than would be predicted from typical body mass scaling patterns.

MATERIALS AND METHODS

Animals

Juvenile blue crabs were collected by sweep-netting in the Cape Fear River at Southport and Wilmington, N.C. and adult animals were purchased locally from fisherman. Animals were acclimated to full strength (1000 mOsmol/L) seawater for approximately one week in an aerated, filtered aquarium. Crabs were fed dried shrimp pellets and frozen blood-worms daily. Prior to sacrifice, animals were sexed and weighed. Carapace width was measured to the nearest millimeter. Only intermolt animals were used, as determined by the rigidity of the carapace, the presence of the membranous layer of the carapace, and the absence of a new, soft cuticle forming beneath the old exoskeleton (Roer and Dillaman, '84).

Succinate dehydrogenase staining

Cell diameter and mitochondrial distribution were examined histochemically by succinate dehydrogenase (SDH) staining and light microscopy. Animals were dissected on ice and the levator branch of the swimming leg muscles (Cochran, '35; White and Spirito, '73; Tse et al., '83) was exposed by removal of the carapace, reproductive and digestive organs, gills, and portions of the endoskeleton. The anterior branch of the levator muscle, which will subsequently be referred to as the light levator due to its pale coloration resulting from low mitochondrial densities (Cochran, '35; White and Spirito, '73; Tse et al., '83), was mechanically isolated from surrounding muscle. The isolated muscle was tied off with 6–0 surgical silk at its origin on the median plate and its insertion at the heavy tendon, which is attached to the antero-dorsal border of the basi-ischiopodite (Cochran, '35). Resting length of the muscle was measured with the fifth pereiopod (swimming leg) positioned as far antero-dorsally as possible so that the levator muscle was in its fully stretched position. The muscle was excised, held at the *in situ* resting length and frozen in isopentane cooled with liquid nitrogen (Tse et al., '83). It was subsequently mounted in gum tragacanth (ICN Biochemicals) and frozen again in cooled isopentane. Samples were stored at -80°C until sectioned. Prior to sectioning, samples were equilibrated to -19°C and 10 μm sections were cut transversely using a Reichert-Jung/Leica Cryocut 1800 and mounted on glass slides. Samples were stained for SDH based on the methods of Nachlas et al. ('57). Slides and nitro-blue tetrazolium (NBT) (Fisher Biotech) were warmed to room temperature for 30 minutes and the staining solution (12.5% solution of NBT in equal volumes of 0.2 M phosphate buffer, pH 7.6, and 0.2 M sodium succinate) was warmed to 37°C. Slides were incubated in the staining solution at 37°C for one hour and gently agitated every five minutes. Areas of high activity turned visibly blue after five minutes while areas of lower activity required the full hour. After the incubation, slides were rinsed at room temperature for two minutes in a 1% NaCl solution and then fixed in a 10% formalin/1% NaCl solution for ten minutes. Slides were dehydrated in 15% ethanol before being mounted in Kaiser's glycerine jelly (Preshnell and Schriebman, '97) and viewed using bright-field optics with an Olympus BH–2 light microscope. Digital images were captured using a Diagnostic Images, Inc. SPOT RT camera and its accompanying software version 3.0.4. The digital images were then analyzed and cell diameters measured using Image-Pro Plus (IPP) version 4.1.0.9 software. The periphery of cells was identified by the areas that stained darkly as a result of the presence of subsarcolemmal mitochondria, and cells were manually outlined with the IPP software. Cell diameters were calculated by an algorithm in the IPP software by taking the average of diameter measurements through the centroid at 2 degree increments around the circumference of a cell.

Transmission electron microscopy

Samples of muscles were analyzed with transmission electron microscopy (TEM) to determine the distribution and density of mitochondria over the range of muscle cell diameters. Animals were dissected as previously described and a small bundle of muscle fibers from the light levator muscle was teased apart with a glass probe. The muscle fiber bundle was isolated as described above and processed based on the methods used by

Egginton and Sidell ('89). Tissue was immediately fixed in a 0.63M Sorenson's phosphate buffer solution containing 1% glutaraldehyde and 4% paraformaldahyde (Preshnell and Schriebman, '97). The osmolarity of the fixative and all corresponding buffer rinses were adjusted by the addition of 10% sucrose and a trace amount of $CaCl_2$ to prevent a change in cell volume and to allow for easy viewing. Tissues were fixed for a minimum of 24 hours at room temperature and rinsed for 15 minutes in Sorenson's phosphate buffer with sucrose and $CaCl_2$. This was followed with a secondary fixation and lipid stain in 1% osmium tetraoxide buffer. Samples were then dehydrated and embedded in Spurr epoxy resin (Electron Microscopy Sciences) and sectioned at 90 nm with a diamond knife on a Reichert Ultracut E. Series of sections were collected using a systematic random sampling method (Howard and Reed, '98) to ensure complete representation of the mitochondrial distribution throughout the muscle. Five sections were collected from a random starting point and then a distance of 500 nm was skipped before collecting another five sections. This process was repeated until 5 μm of tissue was sectioned. Sections were collected and mounted on Formvar-coated (0.25g Formvar in 100mL ethylene dichloride), 200 mesh, high-transmission copper grids. Five micrographs from each of nine samples of muscle from animals ranging in weight from 0.46 to 180 g were collected for a total of 45 micrographs. Samples were stained with 2% uranyl acetate in 50% ethyl alcohol and with Reynolds' lead citrate (Reynolds, '63). Sections were viewed on a Phillips 400 transmission electron microscope operated at 60kV and photographed using a $3'' \times 4''$ plate camera. Micrographs were digitized using a Microtek Scanmaker 4 negative scanner, and the digital images were analyzed with Image-Pro Plus (IPP) version 4.1.0.9 software.

To calculate total fractional area of mitochondria per muscle fiber, stereological point-counting methods were applied (Howard and Reed, '98). A grid of approximately 1,750 points was superimposed on the micrograph and points that fell on either a mitochondria or within a muscle fiber were counted and recorded separately. Points falling extracellularly were not included in the counts. The area associated with each point was multiplied by the number of mitochondrial points to calculate mitochondrial area, and by the total number of points that fell within a muscle fiber to calculate fiber area. The fractional area of mitochondria was determined by dividing mitochondrial area by fiber area. To calculate mean fractional area of mitochondria separated by position within the muscle (i.e. intermyofibrillar or subsarcolemmal), a slightly different stereological method was employed. For these measurements, a grid was applied to each of the 45 micrographs, creating squares with side lengths of 5.2 μm (areas of 27.04 μm^2). Five squares on the grid from each micrograph were randomly selected (for a total of 225 squares from all micrographs), and determined to be either intermyofibrillar or subsarcolemmal based on their distance from the cellular membrane. Squares within 10 μm of the subsarcolemmal membrane were considered subsarcolemmal while those beyond 10 μm were considered intermyofibrillar. Only squares that fell completely on myofibrils were counted, excluding squares that fell between cells or fell partly on the membrane and partly on myofibrils. All mitochondria within each square were counted and recorded. Subsequently, mitochondrial cross sectional area was determined using IPP software. Fifty arbitrarily selected mitochondria from the micrographs of small animals and fifty arbitrarily selected mitochondria from the micrographs of large animals were measured and averaged to calculate an average mitochondrial area. Mitochondria were outlined in the IPP software and the areas within the outlined region were calculated. The mean mitochondrial area was used to determine mitochondrial area of subsarcolemmal and intermyofibrillar mitochondria.

Enzyme assays

Citrate synthase (CS) assays were conducted based on the methods of Walsh and Henry ('90). Tissue was excised and freeze-clamped in liquid nitrogen and stored in plastic vials at $-80^{\circ}C$ until use. Tissue was extracted in 5–20 volumes of enzyme extraction buffer (50 mM Tris, 1 mM EDTA, 2 mM $MgCl_2$, 2 mM DTT, pH 7.6) and sonicated on ice at 10 W in 3 bursts of 5 s each. Samples were centrifuged for 20 min at $16{,}000 \times g$ and the supernant was combined with 1 mM 5,5-dithio-bis [2-nitrobenzoic acid], 0.3 mM acetylcoenzyme A, and water. Absorbance at a wavelength of 412 nm was measured in a Pharmacia Ultraspec 4000 spectrophotometer at $25^{\circ}C$ until the absorbance stabilized. The absorbance change during this period was slight and typically stabilized in 2–3 minutes. The reaction

was initiated by the addition of 0.5 mM oxaloacetate and the enzyme activity was determined from the initial slope of the absorbance change.

Post-contractile glycogen dynamics

To measure the time course of aerobic recovery, burst contractile activity comparable to that during an escape response, was elicited by stimulating the thoracic ring ganglia (Spirito, '72) in vivo. Crabs were removed from the aquaria and suspended in the air with a small clamp so that the swimming leg motion was unrestricted. Small wire electrodes were inserted through two small holes drilled in the mesobranchial region of the dorsal carapace. Animals were stimulated with a Grass Instruments SD9 stimulator at 80 Hz, for 200 ms, at the minimum voltage required to elicit a response (approximately 10V/cm between electrodes). Stimulations elicited a burst-swim response and were repeated a minimum of five times with a 2 s rest between the cessation of swim movement and the next stimulation. Stimulations were stopped when the response of the animal was no longer a burst-swim motion but the slow, sculling motion characteristic of aerobic swimming. Immediately following the procedure, crabs were placed in an aerated aquarium with full-strength seawater and provided with food. The entire stimulation procedure, starting when the animal was removed from the water and ending when the animal was returned to the aquarium, required less than 5 minutes. Crabs remained in the aquaria until they were sacrificed at either 0.5, 1, 2, or 4 h post-exercise. Due to the expected longer recovery period for large crabs (Henry et al., '94) glycogen was also measured at 8 and 24 h post-contraction in the adults. Muscle tissue was excised, freeze-clamped in liquid nitrogen, and ground into a powder before being stored at -80^{o}C. Frozen samples were then analyzed for glycogen based on the methods of Keppler and Decker ('74). Frozen tissue was homogenized in ice-cold 0.6 N perchloric acid with a Fisher Scientific Powergen 125 homogenizer. The homogenate was split into two pools; one for a glucose blank that was used to measure free glucose, and one to measure glycogen. The glycogen hydrolysis pool was neutralized with 1M potassium bicarbonate and incubated for two hours in an amyloglucosidase solution (14 units/mL in 0.2 M acetate buffer, pH 4.8) while shaking at 40°C. After incubation, the reaction was stopped by the addition of 0.6 N perchloric acid and both the glucose blank pool and the glycogen hydrolysis pool were centrifuged at $16{,}000 \times g$ for 10 minutes. Supernatant from both pools was neutralized with 1 M $KHCO_3$ before being assayed. The sample was added to a solution containing 1mM ATP, 0.9 mM β-NADP, 14.7 units glucose–6–phosphate dehydrogenase, 0.3M triethanolamine hydrochloride, and 4.05 mM $MgSO_4$ at pH 7.5. The reaction was started by the addition of 2.75 units hexokinase. The amount of glucose in each pool was proportional to the increase of NADPH, which was measured spectrophotometrically at a wavelength of 340 nM. Subtraction of free glucose in the blank from glucose hydrolyzed from glycogen resulted in a value reflecting μmols of glucosyl units per gram of tissue.

Analysis

One-way analysis of variance (ANOVA) was used to test for main effects of animal size class. Where data were heteroscedastic (Bartlett's test), Welch's ANOVA was used, which accounts for heterogeneous variances. Where significant size effects were detected, Tukey's HSD tests were used to compare means among animal size classes. For glycogen time-series data, t-tests were used to compare post-exercise glycogen concentrations to resting concentrations. All data were analyzed and statistical tests were run with JMP software version 4.0.2. Data are presented as means $\pm$ SEM throughout with a significance accepted at $p < 0.05$.

RESULTS

Histochemistry and cell size

SDH staining clearly showed a dark ring around the outside edge of each muscle fiber, indicative of subsarcolemmal mitochondria (Fig. 1). Mean cell diameter determined from SDH images ranged from 100 to 620 μm in crabs weighing from 0.41 to 231 g, and muscle fiber diameter was directly related to body mass (Fig. 2A). From these data, three animal size classes were created that encompassed muscle fibers with dimensions characteristic of ''normal'' cells (small animal size class), as well as fibers that were giant (medium and large animal size classes) (Table 1; Figs. 1, 2B). Mean cell sizes were significantly different between size animal classes (Fig. 2B). The peripheral ring of mitochondria was darkest and thickest in sections from the large animal size class (Fig. 1C). In juveniles of the small and medium

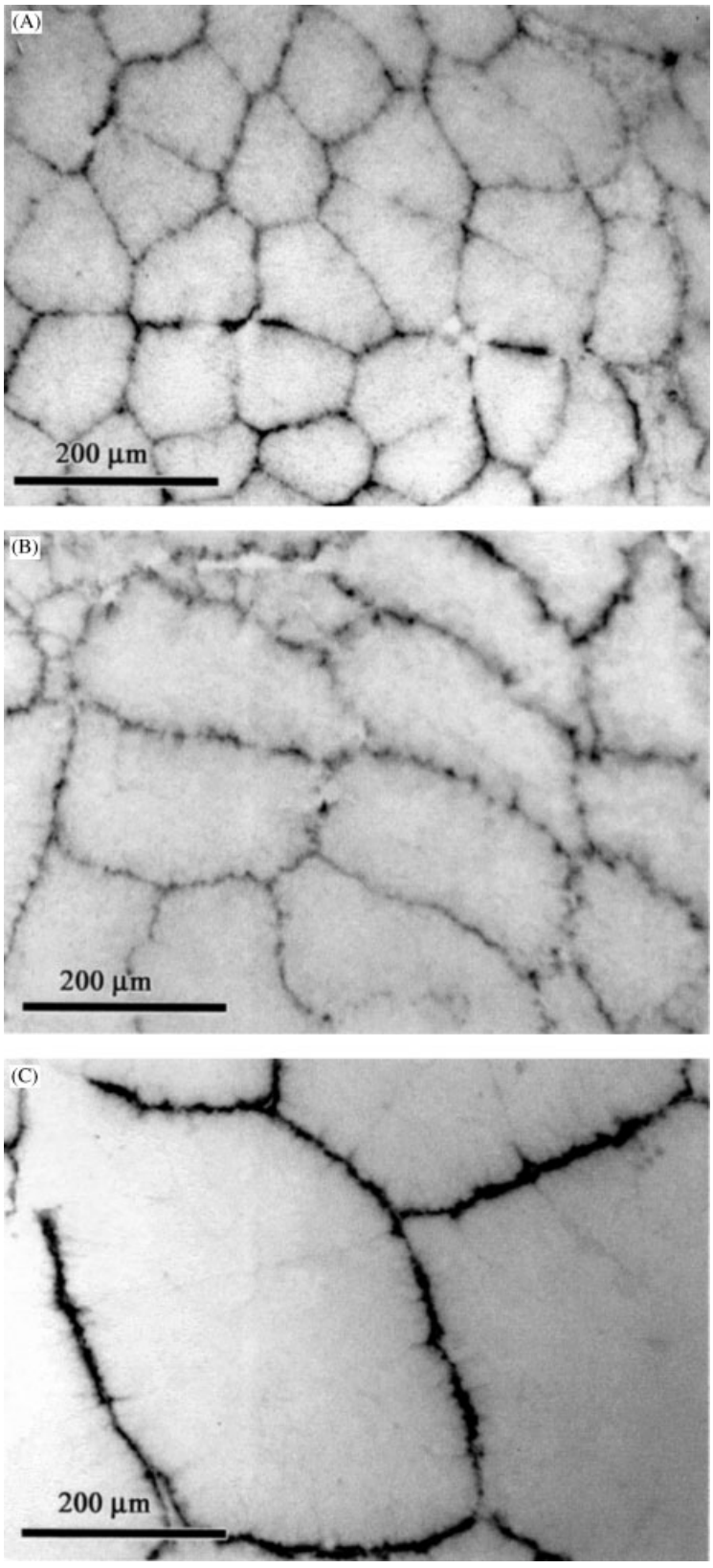

Fig. 1. SDH staining of white levator muscle from (A) small, (B) medium, and (C) large size class animals showing the predominant subsarcolemmal ring of mitochondria and cell size differences. Note the slightly more intense staining within the fiber core of small and medium animal size class and the much greater intensity of staining of subsarcolemmal mitochondria in the large animals.

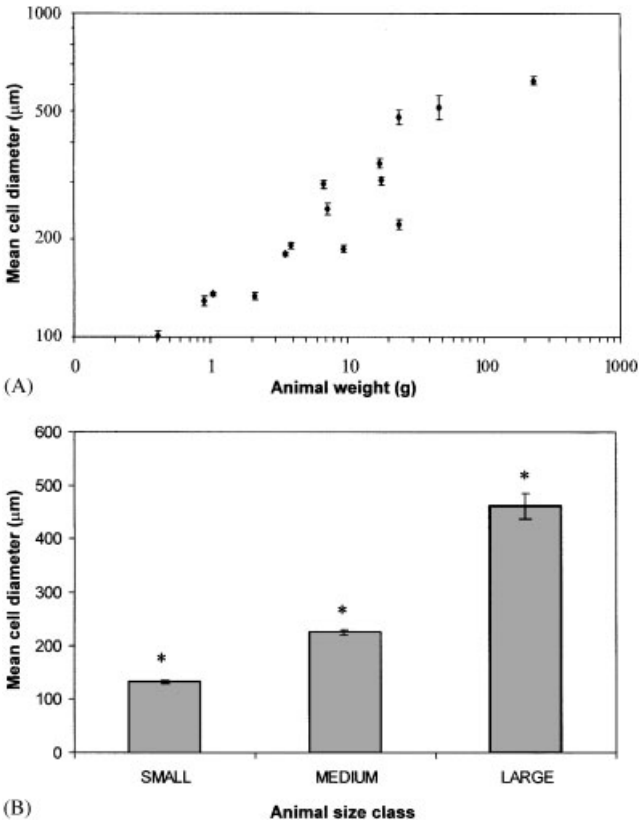

Fig. 2. Cell diameter data. (A) Mean cell diameter plotted against body weight and (B) the same data grouped by animal size class. Each point in (A) represents muscle from an individual animal and N values ranged from 50 cells per muscle in the small animals to 15 cells per muscle in the large animals. In (B) Welch's one-way ANOVA detected a significant size effect ($F=301$, $df=2$, $p<0.05$) and the * indicates mean cell size of each size class was significantly different from that of the other two size classes (Tukey HSD, $p<0.05$). Data are means $\pm$ SEM.

TABLE 1. Summary of size class characteristics for animals used in the SDH histochemical staining experiments. The cell-size data presented in Figure 2 was used to define the three animal size classes that would be used in subsequent experiments. Carapace width and mean weight data are shown as means $\pm$SEM

Animal size class	Mean animal carapace width (mm)	Mean animal weight (g)	Animal weight range (g)
Small (n=5)	23.6 $\pm$ 0.31	1.36 $\pm$ 0.53	0.41–3.50
Medium (n=6)	55.2 $\pm$ 0.535	8.90 $\pm$ 0.299	3.86–17.69
Large (n=4)	101.3 $\pm$ 3.96	109.46 $\pm$ 11.68	23.92–231.26

animal size classes, light staining was visible in the core of the muscle, presumably from intermyofibrillar mitochondria (Fig. 1A,B).

Mitochondrial fractional area and distribution

The size of mitochondria did not change with animal size, as indicated by the fact that the mean cross sectional area of mitochondria was not significantly different among animal size classes (grand mean was 0.608 ± 0.041 μm^2). However, a change in the distribution of mitochondria can be clearly seen and it is apparent that in the large animal size class, mitochondria have a higher subsarcolemmal density than intermyofibrillar density (Fig. 3E,F) while in the small animal size class, mitochondrial densities are comparable in both regions (Fig. 3A,B). In the medium size class, the distribution pattern of mitochondria is intermediate to that of the small and large size classes (Fig. 3C,D). Total fractional area of mitochondria was greater in the large animal size class than in either the medium or small size classes, although this effect was not significant (Fig. 4). When separated based on distribution, a significant effect of animal size class was detected for the mean fractional area of both the subsarcolemmal and intermyofibrillar mitochondrial populations. The subsarcolemmal mitochondrial fractional area increased as animal size class increased, while the opposite effect was observed for the intermyofibrillar fractional area (Fig. 4).

Enzyme activity

Weight-specific citrate synthase activity scaled according to the allometric equation $Y=aM^b$ where Y is CS activity, a is a constant, M is body mass, and b is the scaling exponent (Schmidt-Nielsen, '84). The scaling exponent of CS activity was -0.09 (Fig. 5A). A significant effect of animal size class was detected, and pairwise comparisons indicated that CS activity was significantly lower in the large animal size class than in the small size class (Fig. 5B).

Glycogen use and recovery

All sizes of crabs responded similarly to the electrical stimulus and required the same number of stimulations to elicit fatigue. Although properties of the contractile process were not measured, qualitative observations suggest that the largest animals tended to have bursts of contractions that were of slightly longer duration than the small crabs. However, small crabs exhibited

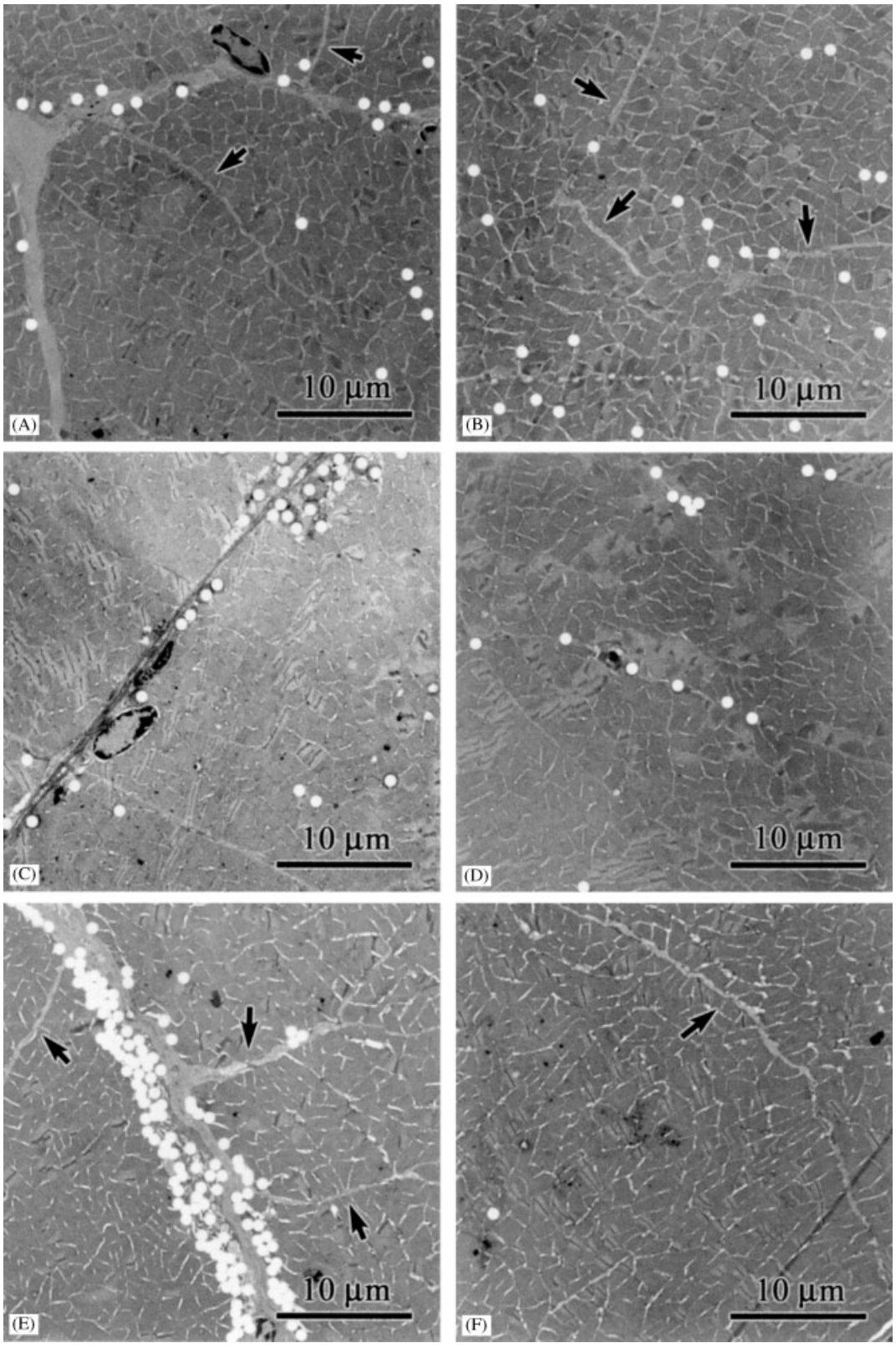
10 µm
(A)
10 µm
(B)
10 µm
(C)
10 µm
(D)
10 µm
(E)
10 µm
(F)

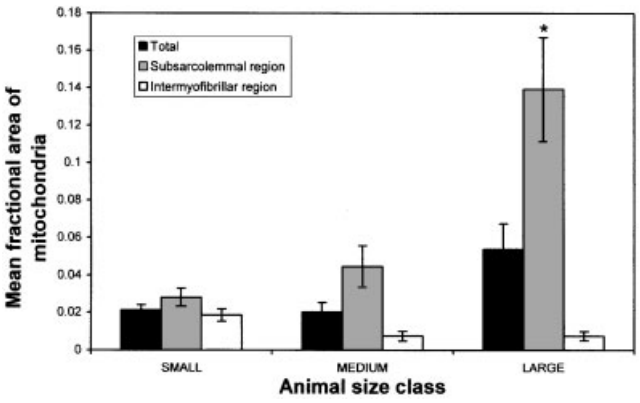

Fig. 4. Mean fractional area of mitochondria for each animal size class. Fractional area is shown as the total across the entire cell, and separated by location into subsarcolemmal or intermyofibrillar regions. Although total fractional area was highest in the large animal size class, Welch's one-way ANOVA did not detect a significant size effect ($F=2.67$, $df=2$, $p=0.077$). A significant effect of size class was detected for both the subsarcolemmal region ($F=8.15$, $df=2$, $p<0.05$) and the intermyofibrillar region ($F=4.25$, $df=2$, $p=0.05$), and the * indicates that in the subsarcolemmal region, the large animal size class had a significantly higher fractional area than the other two size classes (Tukey HSD, $p=0.05$). $N=3$ animals, 15 TEM sections, and 75 counts for each size class (see Material and Methods for clarification). Data are means $\pm$ SEM.

burst-swimming motions at a visibly higher frequency than did larger animals. Animals did not demonstrate any unusual behavioral responses following the stimulation procedure, and a subset of animals that was not sacrificed demonstrated no apparent long-term effects following the treatment.

Glycogen dynamics of each animal size class are illustrated in Fig. 6. The time post-contraction to reach minimum glycogen concentrations increased as animal size increased. In the smallest animal size class (Fig. 6A), the lowest glycogen value was measured at 30 min post-exercise, although the decrease was not significant. The minimum values in the medium and large size classes were significantly different than the resting glycogen concentrations and occurred at 60 and 240 min post-exercise, respectively. In fact, since the largest animal size class still had significantly depressed glycogen concentrations 4 h after contraction, we extended the time course for this group to 24 h. The mean maximum decrease in glycogen concentration following contraction was also proportional to animal size, with the large size animals consuming >3–fold more glycogen than the small size class animals (Figs. 6 and 7).

DISCUSSION

Post-metamorphic blue crabs undergo a 3,000–fold change in body weight during development. With changes in body weight, the anaerobic fibers of swimming leg muscles cross and greatly exceed the 100 μm cell diameter limit that is adhered to by cells of most organisms (Figs. 1 and 2). These changes in fiber dimensions occur despite the fact that the burst-escape function of the muscles remains the same in juvenile and adult crabs. The stimulation procedure used in this study elicited qualitatively similar burst contractions in terms of the number of bursts required to elicit fatigue in animals that ranged from <0.5 to >200 g. Large animals did tend to have bursts of slightly longer duration, however, which is consistent with previous studies of anaerobic contraction in crustaceans (Baldwin et al., '99), although smaller crabs had higher frequencies of contraction. The similar response of this muscle over a wide range of body mass is not unexpected. Anaerobic metabolism should not be greatly affected by giant cellular dimensions because glycolytic pathways are limited by factors contained solely within the cell, such as glycogen concentrations and glycolytic enzyme activities (reviewed in Somero and Childress, '80, '90). However, the low SAV ratios and extreme diffusion distances imposed by giant cell size should create problems for aerobic metabolism due to limited diffusion of oxygen across the sarcolemma and reduced flux of ATP equivalents into the fiber core.

It has been argued that in the case of crustaceans, the SAV limitations imposed by large cells

Fig. 3. TEM micrographs of mitochondrial distributions for each animal size class. Mitochondria are marked with white circles to show distribution. Panels are arranged from top to bottom in order of increasing animal size class. Subsarcolemmal mitochondria are in the left panels and intermyofibrillar mitochondria are in the right panels. (A) Small animal size class subsarcolemmal and (B) intermyofibrillar mitochondria; (C) Medium animal size class subsarcolemmal and (D) intermyofibrillar mitochondria; (E) Large animal size class subsarcolemmal and (F) intermyofibrillar mitochondria. Note the pattern of high densities of subsarcolemmal mitochondria and sparse intermyofibrillar mitochondria in large cells and the relatively similar distribution of subsarcolemmal mitochondria and intermyofibrillar mitochondria in small size class. Also, note that invaginations of the subsarcolemmal membrane have been marked with arrows and that mitochondria are not preferentially associated with the invaginations.

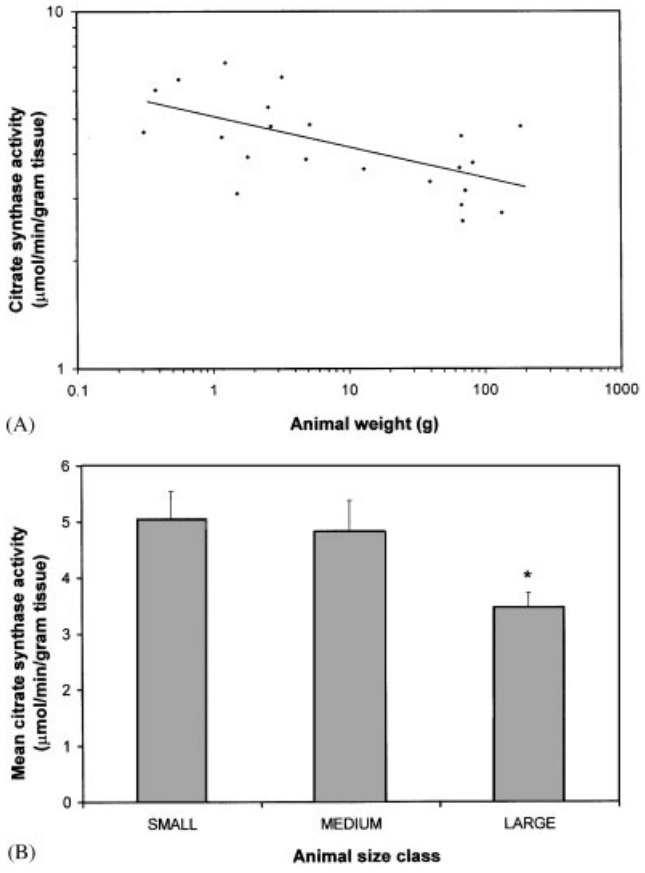

Fig. 5. Weight-specific citrate synthase activity. (A) Citrate synthase activity vs. weight. Note the negative scaling. The line through the data is described by the equation, CS activity=$5.0 \times M^{-0.09}$, where M=body mass (R^2=0.39, p=0.05). (B) Mean citrate synthase activity plotted for each animal size class. In (B) one-way ANOVA detected a significant size effect (F=4.86, df=2, p=0.05) and the * indicates weight-specific citrate synthase activity was significantly different between the large and small animal size class (Tukey HSD, p=0.05). N=8, 5, and 9 for small, medium, and large size classes, respectively. Data are means ± SEM.

are alleviated by the presence of invaginations/clefts in the muscle membrane (Selverston, '67). These clefts are infoldings of the sarcolemma of the cell and extend deep into the intermyofibrillar region of the muscle (Peachy, '67; Selverston, '67; Rossner and Sherman, '78). While these clefts are readily apparent in blue crab fibers, the present study confirmed earlier findings that the mitochondria are virtually absent from the fiber core in the largest cells, meaning the invaginations do not increase the effective metabolic surface area of the cells (Figs. 3 and 4; Tse et al., '83). Thus, since nearly all of the mitochondria are subsarcolemmal in adult muscle, the cells are ''metabolically giant,'' despite the fact that the SAV is increased by sarcolemmal clefts (Fig. 3). It is possible that the increased SAV associated with the sarcolemmal clefts enhances rates of membrane transport, particularly for lactate efflux following burst contraction. However, we consider this effect to be minimal for several reasons. If lactate enters the cleft spaces equally on all sides, the concentration gradient toward the periphery of the cell will be the same as that inside the cell, and thus no increase in peripheral diffusive flux will result from the presence of clefts. The volume of the clefts is also extremely small relative to the fiber volume, meaning that the clefts cannot serve as a quantitatively important reservoir for lactate or other metabolic end products. Further, crustacean giant muscle fibers do not appear to express a lactate transporter (Kinsey and Ellington, 1996) and lactate efflux from crustacean muscle is extremely slow (Milligan et al. 1989; Kinsey and

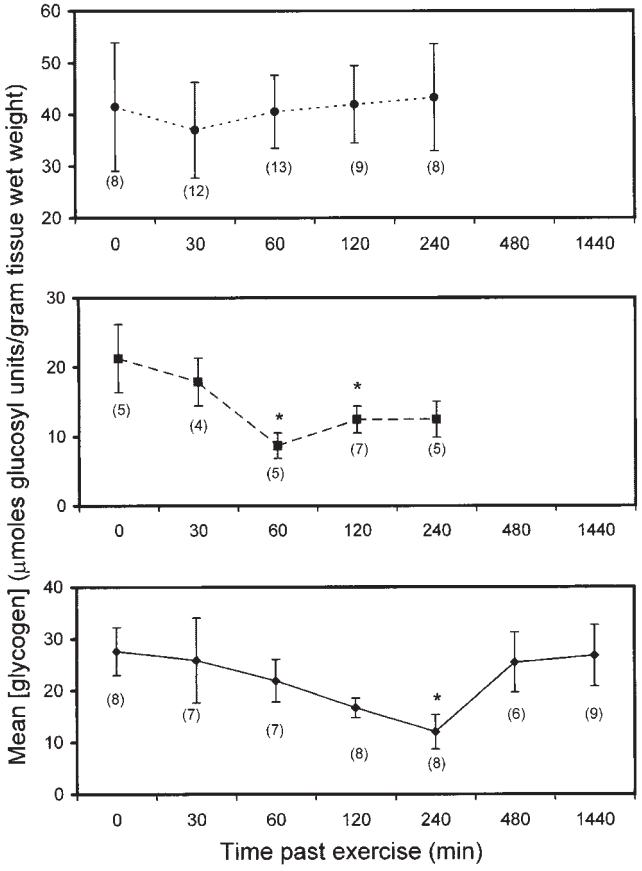

Fig. 6. Changes in glycogen concentration in light levator muscle in (A) small, (B) medium, and (C) large animal size classes. The X-axis represents time post-exercise (exercise occurs at 0 min). The * indicates a significant difference from resting value (0 time point) (t-test, p=0.05). N values for each time are shown below their corresponding point. Data are means ± SEM.

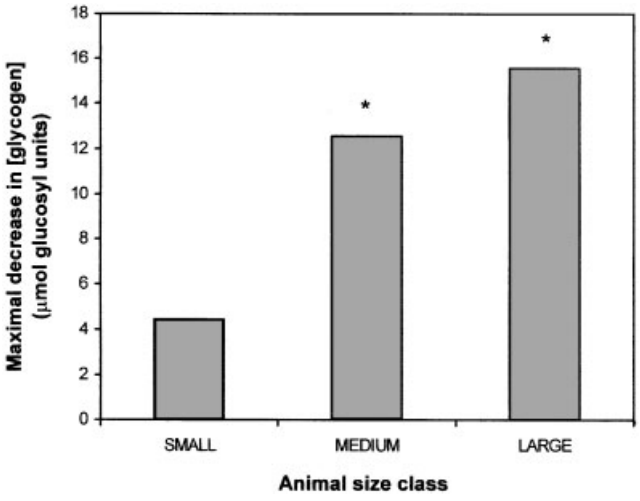

Fig. 7. Maximum decrease in glycogen concentration for each animal size class. These data were derived by subtracting the mean minimum glycogen concentration from the mean resting concentration as shown in Fig. 6, therefore, no error bars can be show for these data. In each case the * indicates a significant decrease from resting values, as shown in Fig. 6.

Ellington, 1996). As originally proposed, the principal, and possibly sole function of these clefts appears to be facilitating electrical propagation to the fiber core during contraction (Peachy, '67; Selverston, '67; Rossner and Sherman, '78).

The changes in mitochondrial distribution with increased cell size were as predicted. In small crabs, mitochondria were found sparsely at the cell periphery and scattered evenly throughout the center of the cell (Figs. 3A,B, 4). In large crabs, a thick ring of subsarcolemmal mitochondria was visible at the fiber periphery, while intermyofibrillar mitochondria were sparse (Figs. 3E,F, 4). This distribution observed in both the SDH stained images and the TEM images, suggests that SAV and diffusion distances dictate the mitochondrial distribution. While it is possible that functions attributed to mitochondria other than the oxygen-dependent production of ATP may determine distribution, there is evidence from other studies that oxygen and ATP-equivalent flux are the dominant controllers. Mainwood and Rakuson ('82) have shown that the clustering of mitochondria near the sarcolemma, coupled with a phosphagen kinase (creatine kinase or arginine kinase) that maintains global equilibrium of high energy phosphate compounds, provides the most efficient flux of both oxygen to mitochondria and ATP equivalents to the fiber core. This arrangement was shown to be superior to a system where mitochondria were evenly distributed throughout the cell, even for nongiant muscle fibers. Kayar et al. ('86) have similarly argued that the predominance of subsarcolemmal mitochondria in muscle of endurance trained rats, as compared to untrained animals, reflects the importance of short diffusion distances for oxygen and other blood-borne substrates, relative to the path lengths for intracellular diffusion of high-energy phosphates between mitochondria and the fiber core. The giant fibers of adult blue crabs represent the extreme case, where oxygen flux to the fiber core is apparently so limited that all of the aerobic potential has been shifted to the fiber perimeter.

Contrary to expectations, the mitochondrial fractional area was higher in muscle from the large animal size class than in the small or medium size classes (Fig. 4). We hypothesized that low SAV and the associated limitations to oxygen flux would lead to a reduction in mitochondrial content with increased body mass that is greater than that expected from typical scaling patterns. However, the shift in mitochondria to the cell periphery in the largest cells was accompanied by a dramatic increase in mitochondrial density in this region (Fig. 4). It is likely that a high peripheral oxidative potential is necessary in the largest cells to maintain the steep concentration gradients of high-energy phosphate compounds that are likely to exist across the cell during post-contractile recovery (Johnston and Maitland, '80).

It is interesting that CS activity, in contrast to mitochondrial fractional area, scaled negatively with increased body size (Fig. 5). Mass specific CS activity typically decreases as body mass increases, but the slope is usually less steep than the slope for mass-specific standard metabolic rate (Somero and Childress, '80, '90; Emmett and Hochachka, '81; Hochachka et al. '88; Childress and Somero, '90). It has been suggested that this discrepancy arises because aerobic enzymes scale according to maximal oxygen consumption, rather than standard metabolic rates (Hochachka et al., '98). However, we predicted that citrate synthase activity would scale more negatively than is typically observed due to limits on aerobic capacity imposed by the extreme cellular dimensions of the fibers. This was not the case, as CS activity had a scaling exponent of -0.09, which is typical of what others have observed in muscle tissue (e.g., Somero and Childress, '80, '90; Emmett and Hochachka, '81). As described above, this prediction was made because the dramatic increase in

the density of subsarcolemmal mitochondria in cells from the largest animal size class was not foreseen. The increased total mitochondrial fractional area (Fig. 4) and decreased citrate synthase activity in large animals further implies that citrate synthase activity per mitochondrion decreases with increasing body (and cell) size.

The predicted functional consequence of having giant cells with a predominance of subsarcolemmal mitochodria is a dramatic reduction in the rate of aerobic processes. It has been previously suggested that post-contraction recovery of glycogen in crustaceans is a slow, aerobic process that is hampered by the modest aerobic scope of crustacean muscle (Booth et al., '82; Booth and McMahon, '92), but the effect of cell size was not considered. In addition, the normally observed negative scaling of aerobic metabolism also leads to the prediction of a reduced rate of aerobic processes as body size increases. Lacking a complete reaction-diffusion model to describe glycogen dynamics, as well as additional pertinent experimental data, a rigorous analysis of the effects of metabolic scaling and giant cell size is not possible. However, the expected impact of these two effects on glycogen recovery can be qualitatively assessed. Normal metabolic scaling would predict that for a 100–fold increase in body mass (the approximate mean difference between our large and small size class; Table 1), specific metabolic rate in the large animal would be 1/3 of that in the small animal ($100^{-0.25}=0.32$) (Schmidt-Nielsen, '84). This suggests that glycogen recovery in large animals should take roughly three times as long as in small animals. Further, our small animal size class differed in body mass from the medium size class by only about 6-fold (Table 1). Thus, the medium size-class crabs would be expected to have a resting metabolic rate that is approximately 2/3 that of the small size class. The differences in post-contractile glycogen dynamics appear to be much more dramatic than predicted by simple scaling, both in terms of the duration of the recovery process and the extent of post-contractile glycogen depletion. In muscle from the small size class animals, there was no significant decrease in glycogen following contraction (Fig. 6A), while in animals from the medium size class, glycogen concentration was significantly lower than resting levels from 1–2 h post-contraction (Fig. 6B). In muscle from the large size class animals, glycogen concentrations were significantly depressed 4 hours after contraction, and recovery to pre-exercise concentrations required approximately 8 hours (Fig. 6C). The time to reach minimum glycogen concentrations and the time required for glycogen recovery reported here were longer than previously reported (Henry et al., '94), presumably because of differences in the exercise regime between studies. The current study focused on short-duration, burst exercise, and not sustained levels of activity as examined by Henry et al. ('94).

Previous studies on crustaceans have reported that glycogen is utilized anaerobically during the recovery from exercise (reviewed by Ellington, '83; Kamp, '89), in contrast to vertebrates, which tend to have a fully aerobic recovery (e.g., Kushmerick, '83; Meyer et al., '84; Meyer, '88; Curtain et al., '97). This anaerobic component of recovery appears to be a strategy to speed up certain phases of the overall recovery process (i.e., AP resynthesis) to allow subsquent contractions (reviewed in Ellington, '83; Thébault et al. '87). In animals from the medium and large size classes of the current study, a substantial amount of glycogen was utilized after exercise. Although the present study cannot determine the extent to which glycogen was oxidized, the similarity of the pattern to other studies and the extent of the decrease suggest that glycogen was used anaerobically and therefore not fully oxidized. This pattern suggests that in larger cells (from the large animal size class), the recovery process has a large anaerobic component, while in the small cells (from the small animal size class) aerobic metabolism may be sufficient to power recovery.

If cellular dimensions and mitochondrial distributions are ignored, the anaerobic contribution to recovery can be examined in terms of oxidative capacity alone. CS activities suggest that oxidative potential is only slightly less in adults than in small juveniles (Fig. 5), while mitochondrial fractional area is actually greatest in the muscle from the largest crabs (Fig. 4). Enzyme activity and mitochondrial density data must be interpreted with caution, but the implication is that aerobic capacity is similar in small and large fibers. It is therefore difficult to reconcile the differences in glycogen dynamics based on typical scaling patterns and aerobic potential without invoking the effects of cellular dimensions and mitochondrial distribution. The protracted recovery and increased reliance on anaerobic glycogen metabolism is, however, consistent with the expected consequences of giant cell size. The fact that medium and large size-class

animals are similar with respect to glycogen recovery (Figs. 6, 7) is not surprising when one considers the fact that muscle fibers from the medium size class are already well above the 100μm threshold. That is, fibers from both the medium and large animal size classes are considered to be ''giant,'' while the small fibers from the smallest crabs are the approximate size of tyical (nongiant) cells (Table 1; Figs. 1, 2). Mainwood and Rakuson ('82) developed a steady-state reaction-diffusion model for a cylindrical cell with only subsarcolemmal mitochondria (which is an accurate representation of a crustacean giant muscle fiber). This model assumes that the AK reaction is always at equilibrium, that the mitochondrial density at the sarcolemma is sufficient to keep pace with local ATP demand, and that ATP is consumed uniformly across the cell, all of which are reasonable assumptions (e.g., Ellington, 2001; Holt and Kinsey, 2002). Figure 8 shows an application of this model based on diffusion distances that are appropriate for the three cell sizes found in each of the three size classes of blue crabs used in this study. In Figure 8A, the steep gradients that exist for AP in large cells even at modest ATPase rates can be observed, while in small cells the gradients are slight. Arginine phosphate transports the vast majority of high-energy phosphate flux in cells with distinct sites of ATP production and consumption (Ellington and Kinsey, '98). Thus, the limiting step in aerobic recovery may be the diffusion of AP from mitochondria at the periphery of the cell to sites in the core of the cell. The time required for a molecule to diffuse a given distance is described by the equation, $t=\lambda^2/2D$, where λ is the displacement in a given direction, D is the diffusion coefficient, and t is the diffusion time. The radial diffusion coefficient of AP in crustacean muscle is 1.0×10^{-6} cm^2/s (Kinsey and Moerland, 2002). Therefore, for a cell with a diameter of 500 μm, it would take AP greater than 5 min to diffuse from the mitochondria at the cell boundary to the fiber core, whereas in cells of typical dimensions phosphagen diffusion from source to sink occurs within several milliseconds.

The AP diffusion gradients in giant cells translate directly to gradients in the effective free energy change of ATP hydrolysis, $dG/d\xi$. The implications of this relationship are shown in Figure 8B. It is clear that in giant cells, even if ATP supply is matched to ATP demand at the

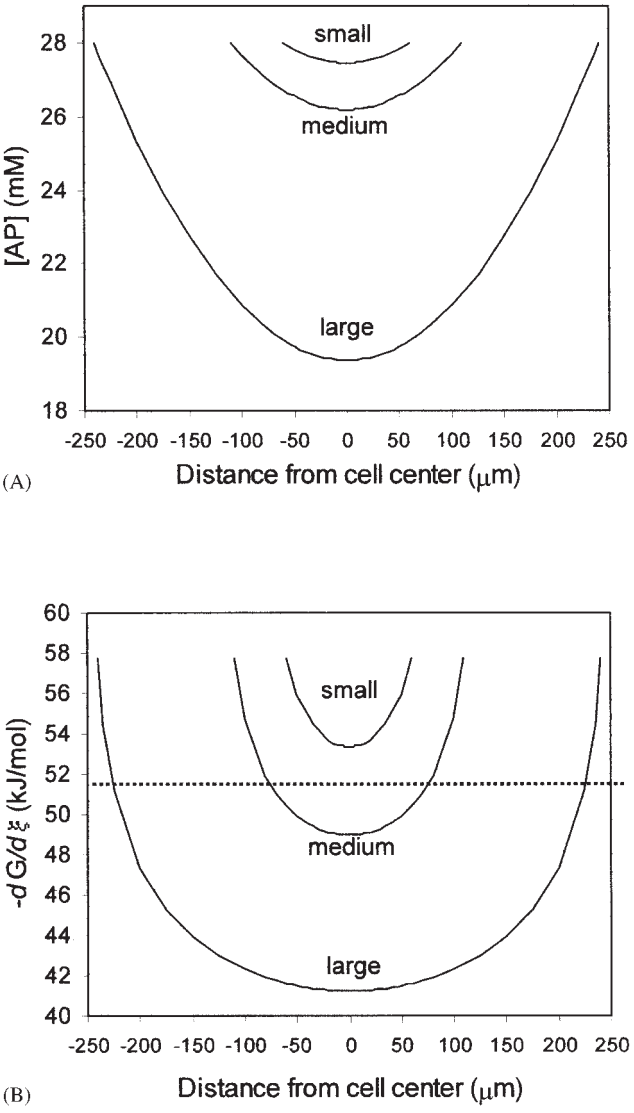

Fig. 8. Examples of expected intracellular gradients during post-contractile recovery in blue crab muscle for (A) arginine phosphate, AP, and (B) the effective free energy of ATP hydrolysis, $dG/d\xi$, using the model of Mainwood and Rakuson ('82). The mean cell sizes from Table 1 for the three animal size classes are plotted (labeled small, medium, and large). In A) the model describes AP concentration profiles in a cylinder with a thin ring of subsarcolemmal mitochondria according to $C_x=C_o - M_p[(R_0^2 - R_x^2)/4D]$ where C_x is the concentration of AP at x distance from the cell center, C_o is the concentration of AP at the cell periphery, M_p is the ATP consumption rate in the fiber core, R_o is the radius of the fiber core (mitochondria to cell center), R_x is the distance from the cell center and D is the diffusion coefficient for AP. Reasonable metabolite concentrations and a modest ATP consumption rate of 10μmol/g/min were used. In B) the $dG/d\xi$ was calculated assuming equilibrium of the AK reaction and an arbitrary threshold of −52 kJ/mol was indicated with the dotted line (Combs and Ellington, 1997).

mitochondria (as the model assumes), aerobic metabolism is probably insufficient to keep up with ATP demand over the entire fiber. Thus, if crustaceans with giant cells relied upon aerobic metabolism alone, even modest rates of ATP demand would cause the $dG/d\xi$ to drop below the threshold levels required for enzyme function. For a given rate of ATP demand, the area of each curve below the threshold illustrated in Figure 8B can be thought of as the extent to which anaerobic metabolism must be relied upon to power the recovery process. The contribution of anaerobic metabolism clearly must be higher in large cells than in small cells, leading to a greater decrease in glycogen concentrations. The fully aerobic components of recovery, such as glycogen resynthesis, must be carried out with a very low rate of ATP demand to prevent the formation of steep concentration gradients. This will lead to a slow aerobic recovery process that is dependent on cell size.

This model assumes a steady-state system, where ATP supply and ATP demand in the fiber core are constant. During recovery, a quasi-steady state likely exists. Immediately after contraction, there will be essentially no AP at the fiber periphery, and the gradients shown in Figure 8 will take time to be established. As recovery progresses the gradients will gradually become less steep. However, the present application of the model is simply to illustrate the dramatic effects of cell size on metabolic recovery, and not to make quantitative predictions regarding rates of recovery.

As mentioned earlier, it has been reported that the ability of crustaceans to perform burst locomotion increases with an increase in body mass (Baldwin et al., '99; Nauen and Shadwick, '99). Although we did not rigorously assess performance, the results of the present study suggest that swimming performance across animal size classes was qualitatively similar. In adult blue crabs, an individual locomotory event was slightly longer and the frequency of leg beating was slower than in small crabs. The increased duration of exercise bursts in the adults may have increased the extent of post-contractile oxygen debt (Head and Baldwin, '86). Although the modest qualitative differences in burst exercise suggest that this effect was minimal, it may be another contribution to the observed differences in glycogen recovery times.

The advantage, if any, conferred by giant muscle fibers in crustaceans is unclear. It is possible that giant fibers exist not because of a functional advantage, but rather because of developmental constraints. Most crustacean muscle grows by increasing the size of existing muscle fibers, rather than the number (Bittner, '68; Lang et al., '70; Bittner and Traut, '78; Mayrand et al., '98), although some fiber proliferation has been observed (Jahromi and Atwood, '71). However, over evolutionary time, crustaceans possess the ability to subdivide these giant, anaerobic fibers into smaller, aerobic functional units, as seen in the dark branches of the levator muscle in swimming crabs (Tse et al., '83). Therefore, if giant fibers were disadvantageous, as they appear to be from a metabolic standpoint, then it seems likely that they would have been eliminated. It is possible that giant fibers may not confer a selective advantage, and their presence may simply reflect the fact that they are not selected against. For instance, it has been shown that as crustaceans grow they rely less on burst swimming for escape and more on defensive behavior (Lang and Govind, '77; Kellie et al., 2001). The adult blue crab is a relatively large animal and it possesses impressive chelipeds and armature. In addition, when pursued, adult blue crabs often engage in highly effective defensive behaviors. Rapid metabolic recovery of muscle following an escape maneuver may therefore not be important to an organism that is highly capable of defending itself. In this light, the metabolic constraints imposed by giant cells may be inconsequential to the organism as a whole. Still, the giant fibers of crustaceans are an outstanding model for studying reaction-diffusion processes and the basis for control of mitochondrial distribution in muscle.

ACKNOWLEDGEMENTS

We thank Dr. Robert Roer, Dr. Ann Pabst and two anonymous reviewers for their many valuable insights. The histochemical and electron microscopy work could not have been completed without the expertise of Mark Gay. We also appreciate the technical assistance of Vicki Stegall.

LITERATURE CITED

Ashley CC. 1967. The role of cell calcium in the contraction of single cannulated muscle fibers. Amer Zool 7:647–659.

Ashley CC. 1978. Calcium ion regulation in barnacle muscle fibers and its relation to force development. Ann N.Y. Acad Sci 307:308–329.

Atwood H. 1973. An attempt to account for the diversity of crustacean muscles. Am Zool 13: 357–358.

Baldwin J, Gupta A, Inglesias X. 1999. Scaling of anaerobic energy metabolism during tail flipping behavior in the

freshwater crayfish, *Cherax destructor*. Mar Fresh Res 50:83–187.
Bittner, GD. 1968. The differentiation of crayfish muscle fibers during development. J Exp Zool 167:439–456.
Bittner GD, Traut DL. 1978. Growth of crustacean muscles and muscle fibers. J Comp Physiol 124:277–285.
Booth CE, McMahon BR. 1985. Lactate dynamics during locomotor activity in the blue crab, *Callinectes sapidus*. J Exp Biol 118:461–465.
Booth CE, McMahon BR. 1992. Aerobic capacity of the blue crab, *Callinectes sapidus*. Physiol Zool 65: 1074–1091.
Booth CE, McMahon BR, Pinder AW. 1982. Oxygen uptake and potentiating effects of increased hemolymph lactate on oxygen transport during exercise in the blue crab, *Callinectes sapidus*. J Comp Physiol 148:111–121.
Childress JJ, Somero GN. 1990. Metabolic scaling: a new perspective based on scaling of glycolytic enzyme activities. Amer Zool 30:161–173.
Cochran DM. 1935. The skeletal musculature of the blue crab, *Callinectes sapidus Rathbun*. Smithsonian Miscellaneous Collections. Vol 92, No. 9, pp 1–76.
Combs CA, Ellington WR. 1997. Intracellular sodium homeostasis in relation to the effective free-energy change of ATP hydrolysis: studies of crayfish muscle fibers. J Comp Physiol B 167: 563–569.
Curtain NA, Kushmerick MJ, Wiseman RW, Woledge RC. 1997. Recovery after contraction of white muscle fibres from the dogfish *Scyliorhinus canicula*. J Exp Biol 200: 1061–1071.
Dorsett DA. 1980. Design and function of giant fibre systems. TINS September 205–208.
Egginton S, Sidell B. 1989. Thermal acclimation induces adaptive changes in subcellular structure of fish skeletal muscle. Am J Physiol 25:R1–R9.
Ellington WR. 1983. The recovery from anaerobic metabolism in invertebrates. J Exp Zool 228: 431–444.
Ellington WR. 2001. Evolution and physiological roles of phosphagen systems. Ann Rev Physiol 63: 289–325.
Ellington WR, Kinsey ST. 1998. Functional and evolutionary implications of the distribution of phosphagens in primitive-type spermatazoa. Biol Bull 195: 264–272.
Emmett B, Hochachka PW. 1981. Scaling of oxidative and glycolytic enzymes in mammals. Resp Physiol 45:261–272.
England WR, Baldwin J. 1983. Anaerobic energy metabolism in the tail musculature of the australian yabby, *Cherax destructor* (crustacea, decopoda, parasacidae): role of phosphagens and anaerobic glycolysis during escape behavior. Physiol Zool 56:614–622.
England WR, Baldwin J. 1985. Anaerobic energy metabolism in the tail musculature of the australian yabby, *Cherax destructor* (crustacea, decopoda, rarastacidae). Regulation of anaerobic glycolysis. Comp Biochem Physiol 80B: 327–335.
Gilbert DL, Adelman WJ, Arnold JM. 1990. Squid as experimental animals. New York: Plenum Press.
Head G, Baldwin J. 1986. Energy metabolism and the fate of lactate during recovery from exercise in the Australian freshwater crayfish *Cherax destructor*. Aus J Mar Fresh Res 37: 641–646.
Henry RP, Booth CE, Lallier FH. 1994. Post-exercise lactate production and metabolism in three species of aquatic and terrestrial decapod crustaceans. J Exp Biol 186:215–234.
Hochachka PW, Emmett B, Suarez, RK. 1988. Limits and constraints in the scaling of oxidative and glycolytic enzymes in homeotherms. Can J Zool 66: 1128–1138.
Holt SM, Kinsey ST. 2002. Osmotic effects on arginine kinase flux in the blue crab, *Callinectes sapdius*. J Exp Biol 205:1775–1785.
Howard CV, Reed MG. 1998. Unbiased sterology, 3–dimensional measurements in microscopy. Oxford, UK: BIOS Scientific Publishers.
Hoyle G. 1987. The giant muscle cells of barnacles. In: Southward AJ, editor. Crustacean Issues 5, Barnacle Biology. Netherlands: A.A. Balkema. p 213–225.
Hoyle G, Smyth Jr. T. 1963. Giant muscle fibers in a barnacle, *Balanus nubuilis* Darwin. Sci 139: 49–50
Johnston IA, Maitland B. 1980. Temperature acclimation in crucian carp, *Carassius carassius*, morphometric analyses of muscle fiber. J Fish Biol 17:113–125
Jahromi SS, Atwood HL. 1971. Electrical coupling and growth in lobster muscle fibers. Can J Zool 49:1029–1034.
Kamp G. 1989. Glycogenolysis during recovery from muscular work. Biol Chem Hoppe-Swyler 370:565–573.
Kayar SR, Claassen H, Hoppeler H, Weibel ER. 1986. Mitochondrial distributions in relation to changes in muscle metabolism in rat soleus. Resp Phys 64:1–12.
Kellie S, Greer J, Cooper RL. 2001. Alterations in habituation of the tail flip response in epigean and troglobitic crayfish. J Exp Zool 290:163–176.
Keppler D, Decker K. 1974. Glycogen determination with amyloglucosidase. In: Bergmeyer HU, editor. Methods of Enzymatic Analysis. New York: Academic Press. p 1127–1131.
Kinsey ST, Ellington WR. 1996. ^{1}H– and ^{31}P–nuclear magnetic resonance studies of L-lactate transport in isolated muscle fibers from the spiny lobster *Panulirus argus*. J Exp Biol 199:2225–2234.
Kinsey ST, Moerland TS. 2002. Metabolite diffusion in giant muscle fibers of the spiny lobster *Panulirus argus*. J Exp Biol 205:3377–3386.
Kushmerick M. 1983. Energetics of muscle contraction. In: Peachy LD, Adrian RH, Geiger SR. editors. Handbook of Muscle Physiology-Skeletal Muscle. Bethesda, MD: American Physiological Society. p 189–236.
Lang F, Govind CK. 1977. Developmental neuroethology: changes in escape and defensive behavior during growth of the lobster. Sci 197:682–685.
Lang F, Sutterlin A, Prosser, CL. 1970. Electrical and mechanical properties of the closer muscle of the Alaskan king crab, *Paralithodes camtschatica*. Comp Biochem Physiol 32: 615–628.
Mainwood GW, Raukusan, K. 1982. A model for intracellular energy transport. Can J Physiol Pharmacol 60:98–102.
Mayrand E, Guderley H, Dutil JD. 1998. Effect of morphometric maturity and size on enzyme activities and nucleic acid ratios in the snow crab, *Chionecetes opilio*. J Crust Biol 18: 232–242.
Meyer RA, Sweeney HL, Kushmerick MJ. 1984. A simple analysis of the 'phosphocreatine shuttle.' Am J Physiol 246:C365–377.
Meyer RA. 1988. A linear model of muscle respiration explains monoexponential phosphocreatine changes. Am J Physiol 254:C548–C553.
Milligan CL, Walsh PJ, Booth CE, McDonald DL. 1989. Intracellular acid-base regulation during recovery from locomotor activity in the blue crab, *Callinectes sapidus*. Physiol Zool 62: 621–638.
Nachlas MM, Tsou K, DeSouza E, Cheng C, Seligman A. 1957. Cytochemical demonstration of succinic dehydrogenase by the use of a new p-nitrophenyl substitute ditetrazole. J Histochm Cytochm 5:420–436.

Nauen JC, Shadwick RE. 1999. The scaling of acceleratory aquatic locomotion: body size and tail-flip performance of the California spiny lobster *Panulirus interruptus*. J Exp Biol 202: 3181–3193.

Newland PL, Neil DM, Chapman CJ. 1992. Escape swimming in the Norway lobster. J Crust Biol 12:342–353.

Peachey LD. 1967. Membrane systems of crab fibers. Am Zool 7:505–513.

Preshnell JK, Schriebman MP. 1997. Humason's Animal Tissue Techniques. Baltimore, MD: John Hopkins University Press.

Reynolds ES. 1963. The use of lead citrate at high pH as an electron opaque stain in electron microscopy. J Cell Biol 17:208–212.

Roer R, Dillaman R. 1984. The structure and calcification of the crustacean cuticle. Amer Zool 24:893–909.

Rosenbluth J. 1969. Sarcoplasmic reticulum of an unusually fast-acting crustacean muscle. J Cell Bio 42:534–547.

Rossner KL, Sherman RG. 1978. Invaginated membrane in crustacean tonic muscle fibers: estimates of membrane capacitance. Am J Physiol 235:C220–C226.

Russell B, Motlagh D, Ashley W. 2000. Form follows function: how muscle shape is regulated by work. J Appl Physiol 88:1127–1132.

Schmidt-Nielsen K. 1984. Scaling: why is animal size so important? New York: Cambridge University Press.

Selverston A. 1967. Structure and function of the transverse tubular system in crustacean muscle fibers. Am Zool 7: 515–525.

Somero GN, Childress JJ. 1980. A violation of the metabolism-size scaling paradigm: activities of glycolytic enzymes in muscle increase in larger-size fish. Physiol Zool 53: 322–337.

Somero GN, Childress JJ. 1990. Scaling of ATP-supplying enzymes, myofibrillar proteins and buffering capacity in fish muscle: relationship to locomotory habitat. J Exp Biol 149: 319–333.

Spirito CP. 1972. An analysis of swimming behaviour in the portunid crab, Callinectes sapidus. Mar Behav Physiol 1:261–276.

Thébault MT, Raffin JP, LeGall JY. 1987. In vivo ^{31}P NMR in crustacean muscles: fatigue and recovery in the tail musculature from the prawn *Palaemon elegans*. Biochem Biophys Res Comm 145:453–459.

Tse FW, Govind CK, Atwood, HL. 1983. Diverse fiber composition of swimming muscles in the blue crab, *Callinectes sapidus*. Can J Zool 61:52–59.

Walsh PJ, Henry RP. 1990. Activities of metabolic enzymes in the deep-water crabs *Chaceon fenneri* and *C. quinquedens* and the shallow-water crab *Callinectes sapidus*. Mar Bio 106: 343–346.

Weiss T, Erxleben C, Rathmayer W. 2001. Voltage-clamp analysis of membane currents and excitation-contraction coupling in a crustacean muscle. J Mus Res Cell Mot 22: 329–344.

White AQ, Spirito CP. 1973. Anatomy and physiology of the swimming leg musculature in the blue crab, *Callinectes sapidus*. Mar Behav Physiol 2:141–153.